Montaser Bakroon, Reza Daryaei, Daniel Aubram, Frank Rackwitz

Investigation of Mesh Improvement in Multimaterial ALE Formulations Using Geotechnical Benchmark Problems

Journal article | **Accepted manuscript (Postprint)**
This version is available at https://doi.org/10.14279/depositonce-10470

This material may be downloaded for personal use only. Any other use requires prior permission of the American Society of Civil Engineers. This material may be found at https://doi.org/10.1061/(asce)gm.1943-5622.0001723

Bakroon, M., Daryaei, R., Aubram, D., & Rackwitz, F. (2020). Investigation of Mesh Improvement in Multimaterial ALE Formulations Using Geotechnical Benchmark Problems. International Journal of Geomechanics, 20(8), 04020114. https://doi.org/10.1061/(asce)gm.1943-5622.0001723

Terms of Use
Copyright applies. A non-exclusive, non-transferable and limited right to use is granted. This document is intended solely for personal, non-commercial use.

WISSEN IM ZENTRUM UNIVERSITÄTSBIBLIOTHEK
Technische Universität Berlin

Investigation of mesh improvement in multi-material ALE formulations using geotechnical benchmark problems

Montaser Bakroon[1] (Corresponding author)
Reza Daryaei[2]
Daniel Aubram[3]
Frank Rackwitz[4]
[1] Research Scholar, Chair of Soil Mechanics and Geotechnical Engineering, Technische Universität Berlin, TIB1-B7, Gustav-Meyer-Allee 25, 13355, Berlin, Germany
[2] Research Scholar, Chair of Soil Mechanics and Geotechnical Engineering, Technische Universität Berlin, TIB1-B7, Gustav-Meyer-Allee 25, 13355, Berlin, Germany
[3] Senior Research Associate, Chair of Soil Mechanics and Geotechnical Engineering, Technische Universität Berlin, TIB1-B7, Gustav-Meyer-Allee 25, 13355, Berlin, Germany
[4] Professor, Head of Chair of Soil Mechanics and Geotechnical Engineering, Technische Universität Berlin, TIB1-B7, Gustav-Meyer-Allee 25, 13355, Berlin, Germany

Abstract

Two of the mesh-based numerical approaches suitable for geotechnical large deformation problems, the multi-material ALE (MMALE) and the Coupled Eulerian-Lagrangian (CEL) methods are investigated. The remeshing step in MMALE is claimed to hold advantages over CEL, but its effects on application problems are not studied in detail. Hence, the possible capabilities and improvements of this step are studied in three large deformation geotechnical problems with soil-structure interaction. The problems are validated and verified using experimental and analytical solutions, respectively. By using the remeshing step in MMALE, a smoother material interface, lower remap-related errors, and better computation cost are achieved.

Keywords

Multi-Material Arbitrary Lagrangian Eulerian, Coupled Eulerian-Lagrangian, large deformations, remeshing, interface reconstruction

Introduction

Small deformation geotechnical problems can be adequately analyzed by using conventional Lagrangian FEM. However, such an approach exhibits considerable shortcomings when the soil undergoes significant deformation. Examples include pile penetration, soil cutting, slope failures, and liquefaction events. Hence, efforts were made to develop methods that simulate the numerical problems associated with large material deformation.

There are various methods to handle such numerical problems which can be categorized into two classes, point-based and mesh-based methods (here only methods derived from continuum mechanics assumption are considered). Examples of point-based methods are material point method (MPM) (Bardenhagen et al., 2000) and smoothed particle hydrodynamics (SPH) (Gingold and Monaghan, 1977), whereas classical FEM (small-strain Lagrangian), Eulerian, ALE, and CEL methods are listed as mesh-based methods (Aubram et al., 2015). Concerning methods that rely on a computational mesh, the most promising approaches include the Coupled Eulerian-Lagrangian (CEL) method and the Arbitrary Lagrangian-Eulerian (ALE) method, which is chosen for this study. The latter can be subdivided into Simplified ALE (SALE) and Multi-Material ALE (MMALE) methods. These methods are popular in fluid dynamics yet not well-known and extensively used in the context of geomechanics. Therefore, the motivation of this paper is to evaluate the possible advantages of MMALE over CEL in case of large deformation geotechnical problems.

Two categories of ALE are generally distinguished, based on a number of materials that might be present in a single element (Fig. 1). Simplified ALE (SALE) approaches resolve material boundaries (free surfaces or material interfaces) in a Lagrangian way using edges and faces (in 3D) of the computational mesh. Therefore, each mesh element is filled with only one material. Unlike SALE, MMALE allows multiple materials to be defined in each element such that material boundaries can flow through the mesh. This method reconstructs the interfaces between multiple materials, making it is suitable to model more complicated and large deforming problem. Fig. 1 provides a schematic comparing all the methods discussed in the present study.

There are various applications of CEL in literature concerned with large deformation problems in geomechanics and geotechnical engineering, e.g., (Bakroon et al., 2019; Heins and Grabe, 2017). One of the earliest works is that done by Qiu et al. (2011), where three numerical benchmarks were used to assess CEL. It was argued that CEL is well suited for large geotechnical problems. Similar conclusions were drawn in a comprehensive and thorough study conducted by Wang et al. (2015) concerning three different numerical approaches, including CEL.

Concurrent to CEL studies, several works were done in applying the ALE method to geotechnical problems. One of the earliest works in application of such similar methods in geotechnical engineering is the “remeshing and interpolation technique with small strain”, RITSS method developed by Hu and Randolph (1998a). In this method, after 10-20 steps of simple infinitesimal strain incremental analysis a rezoning step is performed. Since then, this method is subjected to many improvements and applications such as inclusion of an h-adaptivity rezoning (Hu and Randolph, 1998b) which is then used to simulate pullout test (Song et al., 2008). Similarly, in a series of works done at the university of Newcastle for instance by Nazem et al. (2008) and Sabetamal et al. (2014), an ALE method with coupled formulation was developed to simulate problems such as offshore large deformation problems. In a work done by Aubram et al. (2015), an advanced SALE formulation is implemented, and its performance is evaluated by simulating shallow and pile penetration into the sand. A good agreement between numerical results and experimental measurements was observed.

On the other hand, Bakroon et al. (2018) assessed the feasibility of SALE in large geotechnical deformation problems. It was concluded that for extremely large problems, the SALE exhibits shortcomings, unlike MMALE which converged to a solution. Therefore, MMALE was suggested to be considered as an alternative approach to SALE for solving complex large deformation problems. Consequently, studies focused on applying the MMALE to geotechnical problems.

The structure of this study is as follows. In Section 0, details of the numerical implementation of CEL and MMALE algorithms such as operator splitting, remeshing, and remapping steps, and soil-structure coupling are described. Section 0 presents three numerical examples to investigate the performance of CEL and MMALE, including a discussion of the results. Concluding remarks are provided in Section 0.

Details of MMALE and CEL

The original CEL method was developed by Noh (1964). In this method, the material regions are treated as Eulerian, while the region boundaries are defined as polygons which are then approximated by Lagrangian meshes overlapping the Eulerian mesh. The Eulerian mesh is fixed throughout the analysis. Some commercial codes implemented variants of the original CEL approach. In the particular CEL method used in this study, a Lagrangian step is first conducted which solves the physics of the problem by using a mesh which deforms with the material. In the case of the pure Lagrangian as well as the Lagrangian step in SALE, MMALE, and CEL, employed in this work, the updated Lagrangian (UL)

(Belytschko et al., 2000; Hallquist, 2006) is used. Concerning the utilized objective stress rate, the Jaumann rate is used (Hallquist, 2006; Livermore Software Technology Corporation, 2015).

After performing the Lagrangian step, the mesh is rezoned to its initial configuration to maintain mesh quality (rezoning/remeshing step). Subsequently, the solution is transported from the deformed mesh to the updated/original mesh (remapping/advection step). This method is different than the CEL method developed by Noh (1964) where the Eulerian solution is not divided into a rezone and remap step (Benson, 1992).

The Arbitrary Lagrangian-Eulerian (ALE) method has been developed by Hirt et al. (1974) and Trulio and Trigger (1961) to address the mesh distortion issue attributed to classical Lagrangian approaches. In each ALE calculation cycle, similar to CEL, the general strategy is to perform a three-step scheme consisting of a Lagrangian step, a remeshing (rezone) step, and a remapping step. After the Lagrangian step, the rezone step relocates the nodes of the mesh in such a way that mesh distortion is reduced. Unlike CEL, however, the updated mesh is not necessarily identical to the original mesh but could be obtained through the application of a smoothing algorithm (Donea et al., 2004). Finally, the remapping step transfers the solution variables from the old onto the new (rezoned) mesh.

The focus of this paper is to evaluate the remeshing step in MMALE and CEL as the main distinguishing factor between these methods. The general solving strategy has been discussed in section 0, which is also available in the literature (Benson, 1992).

Therefore, the remeshing step, as well as some other features of MMALE and CEL, are described in this section.

Operator splitting

Generally spoken, operator splitting is a strategy to divide a complicated equation into a sequence of simpler equations (Benson, 1992). Operator splitting can be used to solve the general Eulerian conservation equation:

$$\frac{\partial \phi}{\partial t} + \boldsymbol{\nabla} \cdot \boldsymbol{\Phi} = \boldsymbol{S} \tag{1}$$

Where ϕ is the field variable, $\boldsymbol{\Phi}$ is the flux function, and $\boldsymbol{S}$ is the source term. This equation can be solved whether in one step (Bayoumi and Gadala, 2004; Donea et al., 1982) or alternatively in multiple steps where the equation is broken up into a series of less complicated equations, i.e., into a Lagrangian term ($\frac{\partial \phi}{\partial t} = \boldsymbol{S}$) and a Eulerian term ($\frac{\partial \phi}{\partial t} + \boldsymbol{\nabla} \cdot \boldsymbol{\Phi} = 0$) (Benson, 1992). The schematic view of operator splitting is drawn in Fig. 2.

Remeshing step (Mesh smoothing algorithms)

The main difference between CEL and ALE (SALE and MMALE) emerges when one compares the remeshing (rezoning) step in both methods. In case of remeshing step in CEL, the new mesh is trivially the original mesh at the beginning of the calculation, while in ALE, the remeshing step is performed by using mesh smoothing algorithms that produce a new, less distorted mesh based on the deformed mesh of the Lagrangian step. The new mesh is not necessarily the original mesh of CEL.

To define a robust rezoning algorithm, two criteria must be satisfied. First, the quality of the grid elements must be maintained. Second, the grid should be focused on zones with a rapid variation of material flow to reduce computational errors, which is referred to as the adaptivity control criterion. While these goals seem easy to achieve, they expose a challenge in the derivation of a robust rezoning algorithm. If one considers quality maintenance as the only important factor, then accuracy in areas of high variations will be lost, since pretty similar sizes will be assigned to rezoned grid elements. Algorithms developed merely on this criterion may be strongly dependent on mesh quality, which may not provide a unique solution. Weighting each criterion is therefore difficult, and it may be problem dependent (Knupp et al., 2002).

Rezoning/smoothing techniques can either change the nodal connectivity, such as h-adaptivity where new elements are generated, or keep the nodal connectivity and only relocate the nodes such as r-adaptivity method where the node position are relocated to obtain a smoother mesh (Di et al., 2007). The focus here is to study those smoothing methods where the nodal connectivities are not changed.

Such rezoning algorithms can be divided into different groups, each having its advantages and drawbacks. Coordinate- or grid-based algorithms can be applied to the gird locally or globally. In local coordinate-based algorithms, the nodes are moved based on local criteria (Benson, 1989; Donea et al., 1982). For example, based on neighboring element areas around the node, a ratio of minimum to the maximum area as well as the maximum cosine value of the vertex angles connecting this node to other nodes is calculated. By these two values, the movement requirement of the node will be determined (Benson, 1989). The shortcoming of this method is that it is based on ad hoc quality measures, which means this class of problems is only applicable to a specific group of problems. In addition, there is no guarantee that the resulting mesh is unfolded (Knupp et al., 2002).

An example of a global smoothing algorithm is the one developed by Brackbill and Saltzman (1982), where they modified the Winslow algorithm (Winslow, 1967). Extra terms were added to make the smoothing algorithm stronger. However, the coefficients of such terms are assigned somewhat arbitrary and without a clear guide. In addition, this method is independent of the Lagrangian grid, which makes the resulting mesh, far from the Lagrangian mesh. To resolve this issue, an iterative approximate solution is used. However, it is not guaranteed if the resulting grid is unfolded. Besides, there is no theory to specify the number of iterations by the user (Knupp et al., 2002).

There are numerous studies in remeshing techniques, but to the knowledge of the authors, this step is the least developed aspect of ALE methods. A short description of the three popular methods will be provided.

Volume-weighted smoothing

To better clarify the smoothing methods, Fig. 3 was drawn where the arbitrary node K, is supposed to be rezoned (relocated). Variables subscripted with Greek letters refer to element variables while subscripts with capital letters refer to local node numbering within an element. Also, the letter A is an arbitrary letter corresponding to the nodes of each element adjacent to node K. Therefore in case of the 2D mesh in Fig. 3, A can be *L* or *E*, or *K.*

In volume weighted smoothing, the new position of the node is determined by using the volume of each neighboring element sharing that node. The method is illustrated by Eq. (2) and (3).

First, the nodal coordinates of each element adjacent to node K, $\vec{x}_A$ are averaged using (2) to obtain the coordinate $\vec{x}_\alpha$ (the point is marked with red cross in Fig. 3). The parameter, *N*, corresponds to numbers of element nodes, which can be four or eight for two- and three dimensions, respectively.

The new position of the node K, $\vec{x}\,^{*}_{K}$, is then obtained by the volume-weighted averaging as in Eq. (3) using the volume of each adjacent element, V_α, and the total number of adjacent elements, n_{adj} (Ghosh and Kikuchi, 1991):

$$\vec{x}_{\alpha} = \frac{1}{N}\sum_{A=1}^{N} \vec{x}_{A} \tag{2}$$

$$\vec{x}\,^{*}_{K} = \frac{\sum_{\alpha=1}^{n_{adj}} V_\alpha\, \vec{x}\,^{n}_{\alpha}}{\sum_{\alpha=1}^{n_{adj}} V_\alpha} \tag{3}$$

Laplacian or Simple average smoothing

In this method, the new position of the node K, $\vec{x}\,^{*}_{K}$, will be simply defined based on the averaged position of the N' nodes, $\vec{x}_{\alpha}$, directly connected to K (nodes L in Fig. 3). This means that four nodes are considered in two dimensional quadrilateral meshes and six nodes in three dimensional hexahedral meshes. The new location of node K is thus calculated by,

$$\vec{x}\,^{*}_{K} = \frac{1}{N'}\sum_{j=1}^{N'} \vec{x}_{j} \tag{4}$$

Equipotential smoothing

This method is more complicated than the previous methods and is intended to smooth the whole mesh or a part of it globally. The equipotential method is based on the solution of the Laplace equation (5) associated with the logical, generally curvilinear coordinates representing the grid lines in structured meshes (Winslow, 1963). The concept is to solve (5) for the Cartesian coordinates of the mesh lines, that is x(ξ_i), (i=1, 2, 3) instead of the curvilinear coordinates ξ =(ξ_1, ξ_2, ξ_3), resulting in Eq. (6). In this method, all the element faces which share the node K are considered in the calculation (Nodes L and E in Fig. 3). Therefore, in two dimensions, eight nodes will be studied while in three dimensions, eighteen nodes will be studied (Fig. 3). For more information regarding the calculation process, the reader is advised to see the work done by Souli et al. (2000).

$$\nabla^2 \xi = 0 \tag{5}$$

$$\gamma_1 \partial_{\xi_1\xi_1}\mathbf{x} + \gamma_2 \partial_{\xi_2\xi_2}\mathbf{x} + \gamma_3 \partial_{\xi_3\xi_3}\mathbf{x} + 2\beta_1 \partial_{\xi_1\xi_2}\mathbf{x} + 2\beta_2 \partial_{\xi_1\xi_3}\mathbf{x} + 2\beta_3 \partial_{\xi_2\xi_3}\mathbf{x} = 0 \tag{6}$$

where

$$\gamma_i = \partial_{\xi_i} x_1^2 + \partial_{\xi_i} x_2^2 + \partial_{\xi_i} x_3^2 \quad i = 1, 2, 3, \tag{7}$$

$$\beta_1 = (\partial_{\xi_1}\mathbf{x} \cdot \partial_{\xi_3}\mathbf{x})(\partial_{\xi_2}\mathbf{x} \cdot \partial_{\xi_3}\mathbf{x}) - (\partial_{\xi_1}\mathbf{x} \cdot \partial_{\xi_2}\mathbf{x})\partial_{\xi_3}\mathbf{x}^2 \tag{8}$$

$$\beta_2 = (\partial_{\xi_2}\mathbf{x} \cdot \partial_{\xi_1}\mathbf{x})(\partial_{\xi_3}\mathbf{x} \cdot \partial_{\xi_1}\mathbf{x}) - (\partial_{\xi_2}\mathbf{x} \cdot \partial_{\xi_3}\mathbf{x})\partial_{\xi_1}\mathbf{x}^2 \tag{9}$$

$$\beta_3 = (\partial_{\xi_3}\mathbf{x} \cdot \partial_{\xi_2}\mathbf{x})(\partial_{\xi_1}\mathbf{x} \cdot \partial_{\xi_2}\mathbf{x}) - (\partial_{\xi_3}\mathbf{x} \cdot \partial_{\xi_1}\mathbf{x})\partial_{\xi_2}\mathbf{x}^2 \tag{10}$$

To investigate quantitatively the effectiveness of each smoothing method, a simple numerical model was developed, as shown in Fig. 4. The model consists of nine elements where the upper right node is subjected to a displacement in both horizontal and vertical directions. The left lateral and the lower edge of the model is fixed. An elastic material model is assumed. After displacement, the deformed mesh is evaluated based on the so-called Jacobian distortion index ranging from 0 to 1. This index describes the deviation of the element from its ideal rectangular form. A value close to 1 indicates an element whose shape is close to its ideal form, while a value of 0 indicates a heavily distorted element (Plaxico et al., 2009). In Fig. 4 the distortion index is shown in percentage.

Without using any smoothing method, representing a purely Lagrangian mesh, the deformation is significant in the upper right element and its three adjacent elements. On the other hand, by using the smoothing methods, the distortion is decreased. In this simple example, all smoothing methods provided acceptable results. Another model was also developed where further displacement was applied. In the upper right element, a non-convex element was obtained, and none of the smoothing methods could handle the non-convex element and provided a folded mesh.

Indeed, the present example is too simple to study the performance of each smoothing method thoroughly. The smoothing methods will be later discussed using a benchmark model in section 0.

Remapping step

After generating a new grid, the solution variables have to be transferred to the new mesh. There are several methods to remap the solution from the Lagrangian mesh onto the new mesh (Benson, 1992; Margolin and Shashkov, 2003). Because the mesh topology does not change in both ALE and Eulerian methods, the remap can be stated as an advection problem which can be solved using conservative finite difference or finite volume methods. In such advection algorithms, the difference between the reference and the rezoned grid is interpreted as volume flux, that is, the change of element/cell volume equals the sum of in- and outfluxes across the cell boundary. The updated value of cell-centered solution variables is then determined by calculating the influx and outflux of this variable in each cell using the information of the adjacent cells. Conventionally, each advection algorithm is applied in one coordinate direction and then extended to two or three dimensions using the operator-split technique (Benson 1992; Souli and Benson, 2013).

Another group of remapping algorithms treats the intersection of the reference and rezoned grid as polygons or polyhedra (Berndt et al., 2011; Kucharik and Shashkov, 2012; Margolin and Shashkov, 2003). One of the main differences between these two concepts is the way to treat mixed/multi-material cells. When using advection algorithms, the mixed cells are treated differently than the pure cell, while in intersection-based remapping, both pure and mixed cells are treated alike. For more information about the remapping method based on polygons and polyhedra, the reader is referred to (Berndt et al., 2011; Chazelle, 1989, 1994; Kucharik and Shashkov, 2012; Margolin and Shashkov, 2003).

The current remapping algorithms used in geotechnical engineering are mostly based on advection algorithms. A more detailed description regarding the most utilized advection algorithms, namely the first-order accurate donor cell and second-order accurate Van Leer (MUSCLE) scheme is available the literature (Benson, 1992).

Soil-structure coupling

Almost all problems in geotechnical engineering are characterized by soil-structure-interaction and contact between different materials. Multi-material elements in CEL or MMALE naturally handle contact without contact elements or algorithms (Benson and Okazawa, 2004). These elements use the same velocity for all materials, which is a manifestation of the "no slip" contact condition in mixture theory. However, in many soil-structure-interaction problems, like pile penetration, interfacial slip, and frictional contact play an important role. Moreover, in many situations, the soil undergoes large deformations while deformation of the structure is moderate. Coupling between Lagrangian and non-Lagrangian parts becomes necessary in such cases.

A penalty contact scheme is utilized in most codes owing to its simplicity and robustness. As a simple description, the penalty method applies springs between nodes of Lagrangian and the Eulerian parts. These springs have seeds and anchors. The seeds are attached to the Lagrangian nodes, while anchors are attached to the Eulerian nodes. In practice, it is better to have more nodes in the Lagrangian part interface, to ensure that at least one Eulerian node is tracked by one Lagrangian node. The spring forces are calculated based on the relative penetration of master and slave parts, and the calculated contact spring stiffness.

Numerical Examples

In this section, three application problems are presented which exhibit specific challenges in numerical simulation. Such classical examples are crucial for comparison of different numerical methods since they have a reduced number of complexities. These examples are modeled using MMALE and CEL, and the corresponding results are compared. The comparison includes the calculation time, and the effect of mesh density on it, accuracy in terms of leakage, interface, and energy loss, which will be described during the section. Table 1 lists the comparison criteria and their specific purpose for each numerical example discussed in this section.

For all simulations mentioned in this study, the calculations were carried out in the commercial code, LS-DYNA®, on a server with two 2.93GHz quad-core Intel CPU X5570 processors and 48 GB of RAM. A short description of the element technology and time stepping is provided for completeness. For SALE, 1-point ALE elements are used while for MMALE and CEL, 1-point reduced integration elements are used. Among the various smoothing methods, equipotential smoothing for the MMALE simulations is applied. This smoothing algorithm is commonly used and provides more stable results compared to other methods. For the advection step, van Leer method is chosen over donor cell since it benefits from second-order accuracy (Benson, 1992).

Most CEL and ALE methods use explicit schemes to advance the solution in time. In explicit methods, to maintain stability and acceptable accuracy, an appropriate time step size must be assigned. The critical time step can be estimated by

$$\Delta t_e = \frac{L_s}{c} \tag{11}$$

where L_s is the characteristic length of the element, and c is the sound speed in the corresponding material. Determining a suitable time step size is crucial in geotechnical applications. In MMALE and

CEL methods, the maximum time step size is also restricted by the advection algorithm: the distance of material transport should be less than one element.

Strip footing

The strip footing problem is a well-known benchmark. In this problem, the soil undergoes significant deformation, which challenges the classical Lagrangian methods.

Problem Description

In this problem, large soil deformations are induced by displacement-controlled penetration of a rigid footing. The resulting pressure under the footing can be verified with the analytical solution provided by Hill (1950) using plasticity theory. The footing is initially placed above a container filled with soil. The problem is modeled as plane strain, the lateral boundary nodes of the soil are fixed in the horizontal direction, and the bottom nodes are fixed in the vertical direction. The footing is assumed rigid with smooth (zero friction) sides and a perfectly rough (no slip) base.

Fig. 5 illustrates the initial and boundary conditions of the problem. The strip footing and the soil dimensions are $2 \times 1\ m$ and $4 \times 4\ m$, respectively. Only half of the symmetric problem is modeled. The Tresca failure criterion is adopted according to which plastic deformations occur when shear stresses reach the value $c = 10\ kPa$, the undrained shear strength of the soil. The Poisson's ratio and the Young's modulus are assigned as $v = 0.49$ and $E = 2980\ kPa$, respectively. For the ratio of footing base over soil width = 0.5, the maximum punch pressure for this problem can be calculated from $q_{ult} = 2c(1 + \frac{1}{2}\pi)$ (Hill 1950).

Numerical model consideration

The problem is analyzed using four different methods: Lagrangian, SALE, CEL, and MMALE. The element size in the uniform mesh is 5 cm, with a total number of elements of 3200. The initial mesh configuration is shown in Fig. 5. The footing in all models is simulated as a rigid body. Frictionless penalty contact between the sides of the footing and the soil is defined.

To assess the dependency of results to mesh size, several models with different element sizes were analyzed in another work (Bakroon et al., 2017). The models were solved using SALE method.

Compared to the analytical solution, the optimum mesh size for this problem was reported to be 5 cm. Therefore, 5 cm mesh size is chosen for all the simulations of this problem.

Results

The methods are compared based on pressure results and computation time. A Lagrangian model is also developed to highlight the huge mesh distortion. Fig. 6 shows the pressure results under the footing versus penetration depth for Lagrangian, SALE, CEL, and MMALE compared to the analytical solution. By using the Tresca failure criterion, the pressure should reach a constant value after small penetration. Considering the accuracy of results, the Lagrangian and SALE solution differ from the analytical result by approximately 15% and 10%, respectively. The observed inaccuracy in case of the Lagrangian and SALE can be attributed to several points. The resulting pressure from CEL and MMALE curves follow the same trend as the analytical result, unlike the curves obtained from the Lagrangian and SALE method. It should be noted that initial results included noises which are inevitable in the explicit formulation (Dassault Systèmes, 2016).

One may argue that the error is caused due to the element locking (Heisserer et al., 2007). It should be noted that the reduced integration elements are used, which overrules the possibility of element locking. Another possible reason may be the proximity of the boundaries. Comparing the results obtained from the MMALE and CEL and their accurate results, this argument cannot be valid for this problem. Considering the MMALE and CEL results, the distorted element near the corner should be the cause of this problem.

The resulting deformation for Lagrangian, SALE, CEL, and MMALE analysis is shown in Fig. 7a. During the Lagrangian solution, the mesh is heavily distorted under the corner of the footing and above. Nevertheless, the simulation continued until the termination time. By using SALE, the overall mesh distortion is alleviated. By using different rezoning methods (e.g., volumetric, equipotential, etc.), different meshes are obtained, but no change in pressure results are observed. In SALE, there are still problems associated with areas around the footing corner where the material encounters significant deformation. These elements are still distorted even with the applied rezoning step. In CEL and MMALE, however, since the material can flow through the mesh, this issue is appropriately addressed. In CEL, the initial mesh is maintained while in MMALE, a new arbitrary mesh is generated.

The instantaneous material velocity field at 0.5 m penetration depth is plotted in Fig. 7b. The results of the Lagrangian simulation show a sharp change of the velocity distribution near the lateral boundary of the footing. This is somewhat reduced when using SALE. When using CEL and MMALE, the velocity field is almost uniform in all regions, indicating that the soil particles are moving smoothly counterclockwise from the bottom of the footing to the side and then to the top.

In Fig. 8 the effective plastic strain after penetration is shown, which represents the failure pattern of the soil. Despite the identical pressure results shown in Fig. 6, the MMALE provides a clear failure line under the footing. However, CEL underestimates the failure line by providing a discontinued line. This can be attributed to two improvements done by MMALE. First, more elements are present in the failure area. Second, less advection is conducted in MMALE due to remeshing, which avoids loss in accuracy caused by advection.

The performance of each method also is assessed with regard to computation time. The Lagrangian method requires the least computation time among all methods, while the SALE required the most, about three times more than the classical Lagrangian method. The underlying reason is that in SALE two additional steps, remeshing and remapping, are included in the calculation. Another affecting parameter is the distortion of the elements in areas around the corner of the footing since the minimum time step is controlled by those deformed elements. The simple idea behind the implemented smoothing algorithms reduces mesh quality in such non-convex regions instead of improving it, i.e., the smoothing algorithms become unstable. The CEL and MMALE methods solve the problem much faster than SALE because mesh quality is easily maintained. In other words, the minimum time step size did not change significantly during the calculation, unlike SALE. Compared to calculation time obtained from CEL, MMALE is about 40% faster in spite of an additional rezoning sub-step.

The resulting calculation times above for MMALE were based on the optimal set of solution parameters. By using the default settings, a new mesh is generated, and the solution is remapped after each Lagrangian step, which increases calculation time significantly. In many situations, however, the magnitude of deformation obtained after a time increment is small enough to perform several Lagrangian cycles before executing one rezoning and remapping cycle without affecting results considerably. On the other hand, if the number of Lagrangian cycles before a rezoning and remapping cycle is increased, the magnitude of element distortion may reduce the size of the critical time step, which results in more computation cost. Hence, to reach a minimum computation time, an optimum number of Lagrangian cycles should be assigned. This optimum number is problem-dependent, and no predetermination can be made.

To optimize the computation cost for the strip footing example, six models are developed where the number of Lagrangian cycles before a remap and rezone cycle varies, ranging from 1 to 30 Lagrangian cycles. To highlight the effect of a number of Lagrangian cycles on calculation time, the mesh size was reduced to 2.5 cm, resulting in 12800 elements. The corresponding calculation times in minutes are drawn in Fig. 9. With the default configuration of MMALE (1 Lagrangian cycle per each rezone and remap cycle), the computation cost is about 70 minutes while assigning 10-20 Lagrangian cycles; it is reduced by 70%. For a large number of Lagrangian cycles, on the other hand, reduction of the critical time step through mesh distortion becomes more pronounced, hence calculation time increases.

In this example, by changing the number of Lagrangian cycles, up to 5% change in pressure results was observed. However, for each problem, the accuracy of the results should be checked since they may be affected by a number of Lagrangian cycles.

To investigate this point further, the effect the calculated contact area of the pile with the soil is shown in Fig. 10. In penalty contact method, the contact force is calculated based on the force required to avoid the penetration of the two distinct parts. Generally, this constraint is not adequately maintained and one part "penetrates" or "leaks" inside the other part. In the case of excessive leakage, the contact force will not be accurately computed. To quantitatively investigate this matter, the parameter contact area is used. Theoretically, the value of the contact area should be maintained as of what is calculated at the beginning of the simulation since during the simulation, only the bottom side of the footing is in contact. If this value is increased, it means that leakage has occurred and some of the elements in the second row of the footing has come into contact. In the case of CEL, an increase of 20% in the contact area is observed. On the other hand, by increasing the number of Lagrangian steps to 50, a significant leakage occurs. Nevertheless, values below this number are providing an acceptable range of leakage. This criterion can be hence used as a limiting factor for a proper number of Lagrangian steps.

In addition, one can see the amount of leakage using a parameter referred to as “flux,” which indicates the volume of material passed through the Lagrangian part, in this case, the footing. A high value of flux indicates that a significant volume of material has passed through the Lagrangian part, and therefore, the errors attributed to leakage are significant. This introduces inaccuracies in the simulation. The computed value of flux is shown in Fig. 11 for both MMALE and CEL. As the simulation continues, the cumulated volume leaked through the Lagrangian footing increases with a faster rate for CEL, which indicates a possibly less accurate result for this method.

The effect of mesh size on computation cost for MMALE and CEL is illustrated in Fig. 12 for various cases where the mesh is refined up to 8 times. In addition, the corresponding computation time of advection for each method is drawn. The computation cost of CEL model is normalized to 1 for each case. he remaining computation times (MMALE, advection in MMALE and CEL) are relatively drawn. In all cases, the MMALE is about 20-40% faster. However, the trend is not linear, i.e., in the case of one-fourth of the original size, the computational gain is the least. In all cases of CEL, more than 40% of the time is spent on advection whereas in case of MMALE it is less than about 30%. The underlying reason is the remeshing step, which reduces the advection calculation by providing a mesh which follows the material deformation pattern.

In the context of the numerical modeling, it is desired to keep the mesh as Lagrangian as possible since the advection procedures introduce errors in the calculation, one of which is the loss of kinetic energy during the advection. Typically, the momentum is preferred over the kinetic energy to be conserved during the advection to maintain the monotonicity of the solution. Maintaining both the momentum and kinetic energy is not possible as it invalidates the monotonicity conditions. This leads to kinetic energy loss during the simulation (Souli and Benson, 2013). To compare the performance of MMALE and CEL regarding this matter, the kinetic energy and the loss of kinetic energy are shown in Fig. 13. The use of remeshing results in a reduction of energy less to almost one-fourth of one calculated by CEL. In the case of kinetic energy curves, the one obtained from CEL is oscillating, which may indicate some instabilities in the method compared to the smooth curve of MMALE.

Sand column collapse

The collapse of the sand column on a rigid horizontal plane is an experimental test which has various engineering applications such as determining the angle of repose. In the context of geotechnical engineering, this problem can simply represent problems such as a landslide. In such tests, a column of sand is held in a container, and the holding gate is suddenly released, allowing the sand to collapse by its own weight. For further information regarding sand column theories and experiments see the works done by Doyle et al. (2007); Lube et al. (2007); Staron and Hinch (2007).

Problem Description

An experimental study performed by Lube et al. (2005) has been chosen as a reference model to analyze the robustness of numerical methods. The experimental results of run-out distance and height of the sand column are compared to the obtained numerical values. This problem has been extensively used for performance evaluation of numerical methods such as the work done by Solowski and Sloan (2013). In the experiment, the sand column is placed in a rectangular container. Then, one side of the rectangular container is lifted fast to impose the 2D flow condition. The initial width of the soil column is d_i=0.0905 m with a height to the width aspect ratio (height to width) of 7. The depth of the test soil in a direction normal to flow is 0.2 m. The friction of the horizontal plane (flowing surface) is equal to internal friction of the sand.

Numerical model consideration

Fig. 14 shows the initial configuration of the numerical model. A uniform mesh with an element size of 15 mm is used for the MMALE and CEL simulations. Purely Lagrangian and SALE models were also developed for reasons of comparison. All the models are three-dimensional, defining a slice with one element in a direction normal to the plane. The CEL and MMALE models contain a void region defined to let the soil material flow to these elements after the collapse starts, unlike SALE model where no void elements are needed. Elements with 1-point integration are used, and Mohr-Coulomb is chosen as the material model. Unfortunately, no data regarding the properties of the test sand are reported by Lube et al. (2005). Therefore, the soil properties are assumed as follows, the density, $\rho = 1600\ kg/m^3$, the friction angle, $\phi = 33°$, the dilatancy angle of $\psi = 0$, the cohesion, $c = 0.01\ kPa$, the Poisson's ratio,

$\nu = 0.3$, and the elastic modulus, $E = 840\ kPa$,. The gravity acceleration is 9.806 m/s^2. The left boundary (wall of the container in the experiment) was modeled using a frictionless rigid body part which was removed after the stresses were initialized. The bottom surface was modeled by a rigid body part as well, having tangential penalty friction equal to soil internal friction angle. The run-out distance, as well as the height of the sand column, were measured at different times and compared to numerical results.

Results

To express the shortcomings of the classical simple based formulations against multi-material based formulations, the problem was also simulated with SALE methods. In this case, the mesh became highly distorted, and the calculation stopped. The mesh clearly tracked the material particles, which can be justified by the concentration of mesh elements as shown in Fig. 15. Due to local rezoning inside the material domain, the mesh quality is to some extent uniform, but elements are severely stretched in the horizontal direction due to the constraints imposed by the material boundary on the remeshing capability. Therefore, after reaching approximately 15% of the calculation time, the time step size decreased significantly so that the calculation could not be continued.

In the case of both CEL and MMALE, simulation continued until the final runout distance of the sand column was reached because of the advection technique, i.e., the material can flow through the mesh. Fig. 16 shows that the remeshing capability of MMALE concentrates the mesh in areas of interest, i.e., where the free surface of the sand is located. The newly generated mesh takes the trend of the material movement and deformation. Hence, the resulting interface is smooth, which is not the case when using the CEL method. The difference in concentration of mesh nodes also affects the final shape of the collapsed sand column, i.e., the final interface of MMALE is curved, whereas the interface of CEL is almost linear. The advantage of MMALE over CEL is also highlighted in Fig. 16, where the volume fraction of sand is plotted. In elements completely filled with sand, the volume fraction equals one, which is represented by blue color. Void elements are drawn in red color, and those elements intersected by the free surface are partially filled with sand, thus have a volume fraction between zero and one. MMALE produces an almost smooth interface, whereas the interface obtained with CEL has a stepped shape and is more diffusive. The diffusion thickness of the interface obtained from CEL is about three times more than the one of MMALE. The difference can be attributed to errors caused by remapping. In advection-based remapping methods, only principal directions (normal to element edges) are considered for calculating the advection, neglecting the advection in diagonal directions. Through the MMALE rezoning capability, the element directions are to some extent adjusted to flow directions which results in less remapping errors due to diagonal advection. Moreover, the total advected material volume using an MMALE mesh is usually smaller than for a comparable CEL mesh because the difference between the rezoned mesh and the mesh after the Lagrangian step is reduced.

To compare both methods with the experimental measurements, Fig. 17 is plotted, which draws the shape of the sand regime at several times measured during the experiment and calculated by numerical simulations. During the whole simulation, the obtained run-out distance from CEL is underestimated, which becomes more evident at the further stages of the simulation. On the other hand, the MMALE provides a good agreement in the run-out distance with the experiment. Also, at later stages of the simulation, there is a difference in a sand shape calculated by each method. The final sand shape predicted by MMALE is closer to the experimental values than with CEL.

By evaluating the kinetic energy loss during advection in Fig. 18, Similar to the strip footing problem, the CEL results in about four times more energy loss than MMALE. This may explain the underestimated run-out distance calculated by CEL which highlights the role of the remeshing in addressing the issues associated with complex and high-speed deformation problems.

Nevertheless, the height of the final deformed shape is underestimated, which can be attributed to the employed material model. In any case, the fact that the remeshing step devised in MMALE improved the accuracy, the interface resolution, and the overall deformed shape is highlighted in this problem.

In Fig. 19, the location of several material points tracked through the simulation is drawn. In case of ALE, the displacement of any point would be averaged from the displacement of its neighboring mesh nodes in the element containing the point during the Lagrangian step. In the vertical direction, unlike the horizontal direction, both methods predict the same position. The location of the points near the right side of the column changes more notably. The maximum variation between the calculated positions is attributed to point P4 with almost 30 cm difference. In this point, the change in both horizontal and vertical direction is extreme and in the diagonal direction of the initially generated

Eulerian mesh. By close observation of the final mesh of the MMALE, it is observed that the elements are arranged in a way to capture the movement of the sand column in this direction. Concerning the fact that a considerable amount of particles undergoes such movements, the MMALE may be a better choice over CEL for this problem.

Soil cutting by blade

Soil cutting tests are conventionally used to design cutting blades. Such problems can also be a good indicator of the ability of a numerical approach to treating material separation, which is similar to the case of pile installation. Different semi-empirical relations are available in the literature for predicting the horizontal and vertical cutting force of the blade (McKyes, 1985). However, these relations are often too simple to deliver acceptable results because the complexity of real soil behavior is not adequately modeled (Onwualu, 1998). Moreover, conducting parametric studies using experiments is costly and time-consuming.

Since the material is split during cutting, i.e., new free surfaces are generated, this test is considered as a challenging large deformation problem. In a purely Lagrangian simulation, this would mean that the mesh elements must be separated from each other during the blade progression. Efforts have been made to model such problems using advanced numerical techniques. An application similar to soil cutting by the blade is the penetration of a hollow pile, where the soil is cut by installing the pile.

Problem Description

The test consists of a cutting blade with an inclination angle of 45°, which passes through a body of clay, as shown in Fig. 20. The horizontal component of the cutting blade velocity is initialized from 0 up to 0.04 m/s in the course of two seconds to avoid instant loading, which induces shock load. Afterward, the velocity is kept constant until the end of the solution. The total simulation time is 24 seconds.

Numerical model consideration

The soil model used in the simulation is assigned as an elastic-plastic material employing the von-Mises failure criterion which has a density, $\rho = 2000\ kg/m^3$, the cohesion $c = 50\ kPa$, the Poisson's ratio $\nu = 0.25$, and the elastic modulus of $E = 1000\ kPa$. The parameters are taken from the example in

(Peng et al., 2017) with some modifications. The cutting blade is modeled as a rigid body to minimize the dependency of the model to the blade. The interaction between soil and cutting blade is assigned as a frictionless contact. A uniform mesh size, as shown in Fig. 20 was used with a size of 0.02 m. The model thickness in a perpendicular direction to the plane is 0.05 m. A rather large area of void elements around the elements filled with soil is required to allow the material to flow through the mesh during the cutting process.

Results

As a first step, the problem has been analyzed using the SALE method. In this method, the mesh deforms significantly, and the solution terminates only after the short amount of time since the elements cannot get "out of the way" of the cutting blade (Fig. 21). Consequently, it is not possible to handle such problems using SALE or Lagrangian methods. By contrast, the results obtained with both CEL and MMALE are reasonable. Fig. 22 shows the material deformation after cutting approximately 0.9 m of the soil. It can be seen that these methods pose no restrictions concerning the topological changes in the material domain (material separation) as cutting proceeds. The amount of material penetration into cutting blade elements (so-called material leakage) is limited and can be neglected.

To verify the performance of both methods, a closed-form analytical solution suggested by McKyes (1985) is presented in eqs. (12)-(14) . F_V and F_H, therein are the required vertical and horizontal forces, respectively, to cut the soil. The problem is considered as plane strain. In addition, the tool is considered as smooth and rigid (McKyes, 1985).

$$P = cd\frac{cot\phi}{sin\alpha}\left[\left(\frac{1+sin\phi}{1-sin\phi}\right)e^{(2\alpha-\pi)tan\phi}-1\right]+qd\left(\frac{1+sin\phi}{1-sin\phi}\right)\frac{e^{(2\alpha-\pi)tan\phi}}{sin\alpha} \tag{12}$$

$$F_H = Psin(\alpha+\phi)+cdcot\alpha \tag{13}$$

$$F_V = Pcos(\alpha+\phi)-cd \tag{14}$$

Where P is the total force per unit width, c is the cohesion, and d is the cutting depth. Other parameters are shown in Fig. 23. Using the c = 50 kPa, d = 0.25 m, $\phi \approx 0°$, $\alpha = 45°$, q = 0 kPa, and considering the model width of 0.05 m, the forces are calculated as $F_H = 893\ N$ and $F_V = 356\ N$.

Fig. 24 shows the vertical and horizontal forces induced on the cutting blade for both CEL and MMALE, as well as the analytical solution. By assigning the same material model, both methods converge to a similar value. Compared to the analytical solution, the horizontal and vertical forces from both methods are in good agreement.

As a verification measure, internal and kinetic energy were checked. As a rule of thumb, the kinetic energy of the deforming material should not exceed the range of 5% to 10% of internal energy during the simulation (Dassault Systèmes, 2016).

The internal energy in both MMALE and CEL converge to the same value (Fig. 25); however, in CEL, a sudden jump is observed. Also, a sudden increase is observed in kinetic energy in CEL. Considering the quasi-static condition of the problem, it is unlikely that such sudden variations possibly occur during the simulation. Therefore, it can be argued that MMALE provides more stable and smoother results. Nevertheless, the tolerance for internal to kinetic energy ratio is still in the range of 5% for both methods.

In this problem, the same mesh size is used in both methods. Due to the quasi-static condition applied to the model, the amount of distortion at each time step is limited, which makes it possible to increase the number of a Lagrangian cycle per rezone step in MMALE. The optimized computation cost of MMALE was then almost half of CEL.

Summary and Conclusions

In this research, the effect of the remeshing step in MMALE is evaluated and compared against CEL, a particular case of MMALE where no remeshing is performed. The evaluation is based on the calculation cost optimization, accuracy, and stability. Three large deformation problems were presented and discussed, for which experimental or analytical results are available. By using the remeshing step, the following points were observed in those problems:

- Computation cost optimization can be performed by modifying a number of Lagrangian cycles before a rezone and remap cycle. Therefore, in these cases about 20 - 40% reduction in calculation time, can be achieved. This is not the case in CEL, as shown in the strip footing and soil cutting problem.

- Using the MMALE, a better accuracy can be achieved compared to the CEL, for instance in the example of a sand column collapse, the error in the predicted run-out distance calculated by MMALE was 2% while in the case of CEL it was about 20%.
- Due to the consideration of the material motion, the remeshing step helps to reach a better resolution of the material interface, as shown in the example of a sand column collapse where the diffusion thickness of the interface was three times less than CEL.
- Owing to the remeshing step in MMALE less remap-related errors, including energy loss during advection and material leakage which deteriorate the simulation results, are produced, and better stability is achieved since less volume is transported during the remap step. In the case of the strip footing about 70% less energy loss and 30% less leakage was observed.

Finally, it can be concluded that MMALE is suitable, though the highly sophisticated numerical method for applications in geotechnical engineering involving large material deformations and topological changes of the material domain.

The problems discussed here were modeled using simple material constitutive equations. Further investigations are required to assess the performance of more complex material models in conjunction with MMALE. Moreover, the multi-phase simulation, such as the inclusion of pore water pressure has not been performed using MMALE element formulation. Further studies regarding problems with various drainage conditions are needed.

Data Availability

Data in graphs generated or used during the study are available from the corresponding author by request.

Acknowledgments

The authors are thankful for the partial financial support obtained from Deutscher Akademischer Austauschdienst (DAAD) with grant number 91561676 and the Elsa-Neumann scholarship of city Berlin (NAFOEG) with grant number T68001.

References

Aubram, D., Rackwitz, F., Wriggers, P., and Savidis, S. A. (2015). “An ALE method for penetration into sand utilizing optimization-based mesh motion." *Computers and Geotechnics*, Elsevier Ltd, 65, 241–249.

Bakroon, M., Daryaei, R., Aubram, D., and Rackwitz, F. (2017). "Arbitrary Lagrangian-Eulerian Finite Element Formulations Applied to Geotechnical Problems." *Numerical Methods in Geotechnics*, J. Grabe, ed., BuK! Breitschuh & Kock GmbH, Hamburg, Germany, 33–44.

Bakroon, M., Daryaei, R., Aubram, D., and Rackwitz, F. (2018). "Multi-Material Arbitrary Lagrangian-Eulerian and Coupled Eulerian-Lagrangian methods for large deformation geotechnical problems." *Numerical Methods in Geotechnical Engineering IX: Proceedings of the 9th European Conference on Numerical Methods in Geotechnical Engineering (NUMGE 2018)*, A. S. Cardoso, J. L. Borges, P. A. Costa, A. T. Gomes, J. C. Marques, and C. S. Vieira, eds., CRC Press, Porto, Portugal, 673–681.

Bakroon, M., Daryaei, R., Aubram, D., and Rackwitz, F. (2019). "Numerical evaluation of buckling in steel pipe piles during vibratory installation." *Soil Dynamics and Earthquake Engineering*, 122, 327–336.

Bardenhagen, S. G., Brackbill, J. U., and Sulsky, D. (2000). "The material-point method for granular materials." *Computer Methods in Applied Mechanics and Engineering*, 187(3–4), 529–541.

Bayoumi, H. N., and Gadala, M. S. (2004). "A complete finite element treatment for the fully coupled implicit ALE formulation." *Computational Mechanics*, 33(6), 435–452.

Belytschko, T., Liu, W. K., and Moran, B. (2000). *Nonlinear finite elements for continua and structures*. John Wiley, Chichester.

Benson, D. J. (1989). "An efficient, accurate, simple ale method for nonlinear finite element programs." *Computer Methods in Applied Mechanics and Engineering*, 72(3), 305–350.

Benson, D. J. (1992). "Computational methods in Lagrangian and Eulerian hydrocodes." *Computer Methods in Applied Mechanics and Engineering*, 99(2–3), 235–394.

Benson, D. J., and Okazawa, S. (2004). "Contact in a multi-material Eulerian finite element formulation." *Computer Methods in Applied Mechanics and Engineering*, 193(39-41 SPEC. ISS.), 4277–4298.

Berndt, M., Breil, J., Galera, S., Kucharik, M., Maire, P. H., and Shashkov, M. (2011). "Two-step hybrid conservative remapping for multimaterial arbitrary Lagrangian-Eulerian methods." *Journal of Computational Physics*, Elsevier Inc., 230(17), 6664–6687.

Brackbill, J. U., and Saltzman, J. S. (1982). "Adaptive zoning for singular problems in two dimensions." *Journal of Computational Physics*, 46(3), 342–368.

Chazelle, B. (1989). "An optimal algorithm for intersecting three-dimensional convex polyhedra." *30th Annual Symposium on Foundations of Computer Science*, 21(4), 671–696.

Chazelle, B. (1994). "Computational geometry: a retrospective." *Proceedings of the twenty-sixth annual ACM symposium on Theory of computing - STOC '94*, ACM Press, New York, New York, USA, 75–94.

Dassault Systèmes. (2016). "Abaqus: Version 2016 documentation."

Di, Y., Yang, J., and Sato, T. (2007). "An operator-split ALE model for large deformation analysis of geomaterials." *International Journal for Numerical and Analytical Methods in Geomechanics*, 31(12), 1375–1399.

Donea, J., Giuliani, S., and Halleux, J. P. (1982). "An arbitrary lagrangian-eulerian finite element method for transient dynamic fluid-structure interactions." *Computer Methods in Applied Mechanics and Engineering*, 33(1–3), 689–723.

Donea, J., Huerta, A., Ponthot, J.-P., and Rodríguez-Ferran, A. (2004). *Arbitrary Lagrangian-Eulerian Methods*. *Encyclopedia of Computational Mechanics*, John Wiley & Sons, Ltd, Chichester, UK.

Doyle, E. E., Huppert, H. E., Lube, G., Mader, H. M., and Sparks, R. S. J. (2007). "Static and flowing regions in granular collapses down channels: Insights from a sedimenting shallow water model." *Physics of Fluids*, 19(10), 16.

Ghosh, S., and Kikuchi, N. (1991). "An arbitrary Lagrangian-Eulerian finite element method for large deformation analysis of elastic-viscoplastic solids." *Computer Methods in Applied Mechanics and Engineering*, 86(2), 127–188.

Gingold, R. A., and Monaghan, J. J. (1977). "Smoothed particle hydrodynamics: theory and application to non-spherical stars." *Monthly Notices of the Royal Astronomical Society*, 181(3), 375–389.

Hallquist, J. (2006). *LS-DYNA® theory manual*. *Livermore Software Technology Corporation*, Livermore Software Technology Corporation, California.

Heins, E., and Grabe, J. (2017). "Class-A-prediction of lateral pile deformation with respect to vibratory and impact pile driving." *Computers and Geotechnics*, 86, 108–119.

Heisserer, U., Hartmann, S., Düster, A., and Yosibash, Z. (2007). "On volumetric locking-free behaviour of p-version finite elements under finite deformations." *Communications in Numerical Methods in Engineering*, 24(11), 1019–1032.

Hill, R. (1950). *The Mathematical Theory of Plasticity*. Oxford Classic Texts in the Ph, Clarendon Press.

Hirt, C. W., Amsden, A. A., and Cook, J. L. (1974). "An Arbitrary Lagrangian-Eulerian Computing Method for All Flow Speeds." *Journal of Computational Physics*, 14, 227–253.

Hu, Y., and Randolph, M. F. (1998a). "A practical numerical approach for large deformation problems in soil." *International Journal for Numerical and Analytical Methods in Geomechanics*, 22(5), 327–350.

Hu, Y., and Randolph, M. F. (1998b). "H-adaptive FE analysis of elasto-plastic non-homogeneous soil with large deformation." *Computers and Geotechnics*, 23(1–2), 61–83.

Knupp, P., Margolin, L. G., and Shashkov, M. (2002). "Reference Jacobian Optimization-Based Rezone Strategies for Arbitrary Lagrangian Eulerian Methods." *Journal of Computational Physics*, 176(1), 93–128.

Kucharik, M., and Shashkov, M. (2012). "One-step hybrid remapping algorithm for multi-material arbitrary Lagrangian-Eulerian methods." *Journal of Computational Physics*, Elsevier Inc., 231(7), 2851–2864.

Livermore Software Technology Corporation. (2015). *LS-DYNA® Keyword user's manual*. Livermore, California.

Lube, G., Huppert, H. E., Sparks, R. S. J., and Freundt, A. (2005). "Collapses of two-dimensional granular columns." *Physical Review E - Statistical, Nonlinear, and Soft Matter Physics*, 72(4), 41301.

Lube, G., Huppert, H. E., Sparks, R. S. J., and Freundt, A. (2007). "Static and flowing regions in granular collapses down channels." *Physics of Fluids*, 19(4), 9.

Margolin, L. G., and Shashkov, M. (2003). "Second-order sign-preserving conservative interpolation (remapping) on general grids." *Journal of Computational Physics*, 184(1), 266–298.

McKyes, E. (1985). "Soil cutting and tillage." *Developments in Agricultural Engineering*, Developments in agricultural engineering, Elsevier, Amsterdam.

Nazem, M., Sheng, D., Carter, J. P., and Sloan, S. W. (2008). "Arbitrary Lagrangian–Eulerian method for large-strain consolidation problems." *International Journal for Numerical and Analytical Methods in Geomechanics*, 32(9), 1023–1050.

Noh, W. F. (1964). "CEL: A TIME-DEPENDENT, TWO-SPACE-DIMENSIONAL, COUPLED EULERIAN-LARGIAN CODE." *Methods in Computational Physics*, B. Alder, S. Fernbach, and M. Rotenberg, eds., Academic Press Inc., New York and London, 393.

Onwualu, A. (1998). "Draught and vertical forces obtained from dynamic soil cutting by plane tillage tools." *Soil and Tillage Research*, 48(4), 239–253.

Peng, C., Zhou, M., and Wu, W. (2017). "Large Deformation Modeling of Soil-Machine Interaction in Clay." *Geomechanics and Geoengineering*, Springer, 249–257.

Plaxico, C., Miele, C., Kennedy, J., Simunovic, S., and Zisi, N. (2009). *U08 : Finite Element Analysis Crash Model of Tractor-Trailers (Phase B)*. Knoxville, Tennessee.

Qiu, G., Henke, S., and Grabe, J. (2011). "Application of a Coupled Eulerian-Lagrangian approach on geomechanical problems involving large deformations." *Computers and Geotechnics*, Elsevier Ltd, 38(1), 30–39.

Sabetamal, H., Nazem, M., Carter, J. P., and Sloan, S. W. (2014). "Large deformation dynamic analysis of saturated porous media with applications to penetration problems." *Computers and Geotechnics*, Elsevier Ltd, 55, 117–131.

Solowski, W. T., and Sloan, S. W. (2013). "Modelling of sand column collapse with material point method." *Proceeding of the Third International Symposium on Computational Geomechanics (ComGeo III)*, S. P. Gyan Pande, ed., Krakow, Poland, 698–705.

Song, Z., Hu, Y., and Randolph, M. F. (2008). "Numerical Simulation of Vertical Pullout of Plate Anchors in Clay." *Journal of Geotechnical and Geoenvironmental Engineering*, 134(6), 866–875.

Souli, M., and Benson, D. J. (2013). *Arbitrary Lagrangian-Eulerian and Fluid-Structure Interaction*. *Arbitrary Lagrangian-Eulerian and Fluid-Structure Interaction*, (M. Souli and D. J. Benson, eds.), John Wiley & Sons, Inc., Hoboken, NJ USA.

Souli, M., Ouahsine, A., and Lewin, L. (2000). "ALE formulation for fluid–structure interaction problems." *Computer Methods in Applied Mechanics and Engineering*, 190(5–7), 659–675.

Staron, L., and Hinch, E. J. (2007). "The spreading of a granular mass: Role of grain properties and initial conditions." *Granular Matter*, 9(3–4), 205–217.

Trulio, J., and Trigger, K. R. (1961). *Numerical Solution of the One-Dimensional Hydrodynamic Equations in an Arbitrary Time-Dependent Coordinate System. Report UCRL-6522*. Livermore, USA.

Wang, D., Bienen, B., Nazem, M., Tian, Y., Zheng, J., Pucker, T., and Randolph, M. F. (2015). "Large deformation finite element analyses in geotechnical engineering." *Computers and Geotechnics*, Elsevier Ltd, 65(April), 104–114.

Winslow, A. M. (1963). *Equipotential zoning of two-dimensional meshes (UCRL-7312)*. United States.

Winslow, A. M. (1967). "Numerical Solution of the Quasilinear Triangle." *Journal of Computational Physics*, 2, 149–172.

Tables

Table 1: Comparison criteria and their purpose for the numerical examples

Application	Criterion	Purpose	Ref. No.
Strip footing (Section 0)	Induced pressure under the footing	Quantitative comparison with an analytical solution	Fig. 6
	Mesh distortion	Qualitative comparison of mesh quality maintenance	Fig. 7a
	Velocity field in the soil	Qualitative comparison of the uniformity in the velocity field	Fig. 7b
	Effective plastic strain	Qualitative comparison according to engineering judgment	Fig. 8
	Number of Lagrangian cycles in MMALE	Calculation time optimization without deterioration in the results	Fig. 9
	Contact area	Quantitative comparison with the ideal contact area	Fig. 10
	Flux/Leakage	Quantitative comparison with ideal zero leakage	Fig. 11
	Relative computation cost	Evaluation of remeshing and advection effects	Fig. 12
	Mesh density	Evaluation of the effects concerning the increase in the calculation time	Fig. 12
	Energy loss	Quantitative comparison with zero energy loss	Fig. 13
Sand column 0)	Mesh distortion	Qualitative comparison of mesh quality maintenance	Fig. 15
	Interface reconstruction	Qualitative comparison of improvement in interface reconstruction	Fig. 16
	Run-out distance	Quantitative comparison with experimental measurement	Fig. 17
	Energy loss	Quantitative comparison with zero energy loss	Fig. 18
	Particle trajectories	Quantitative comparison of soil particle flow and evaluation of methods in capturing complex material movement	Fig. 19

	Calculation time	Evaluation of the effect of remeshing in the reduction of calculation time	0
Soil cutting (Section 3.3)	Mesh distortion	Qualitative comparison of mesh quality maintenance	Fig. 21 Fig. 22
	Induced vertical and horizontal forces on the blade	Quantitative comparison with an analytical solution	Fig. 24
	Internal and kinetic energy time histories	Qualitative comparison of the convergence of the results; verification of the steady state condition	Fig. 25
	Calculation time	Evaluation of the effect of remeshing in the reduction of calculation time	Section 0

Figures

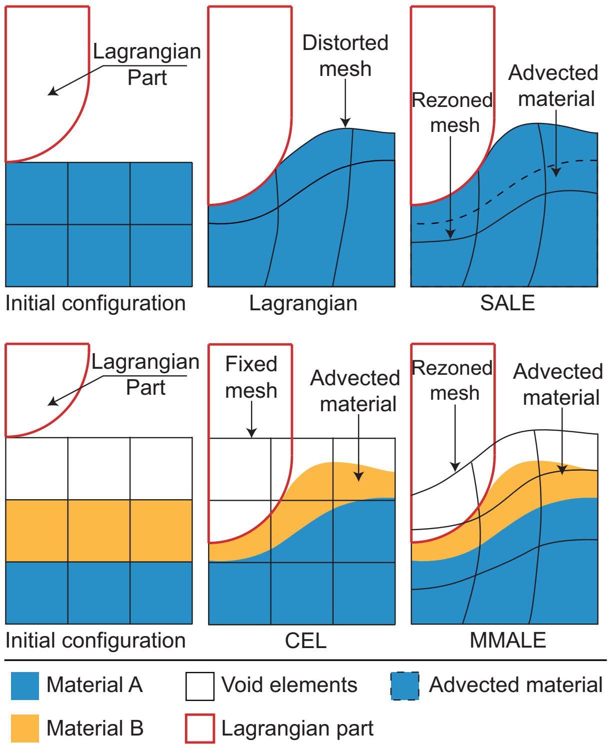

Fig. 1 Schematic diagram of different grid-based approaches comparing the remeshing step effects on grid distortion level.

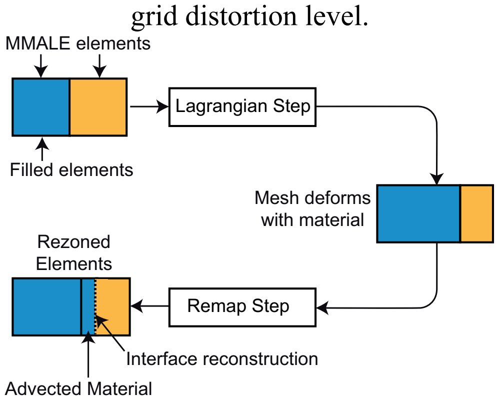

Fig. 2 Flowchart of the operator split scheme applied to the CEL and MMALE calculation steps

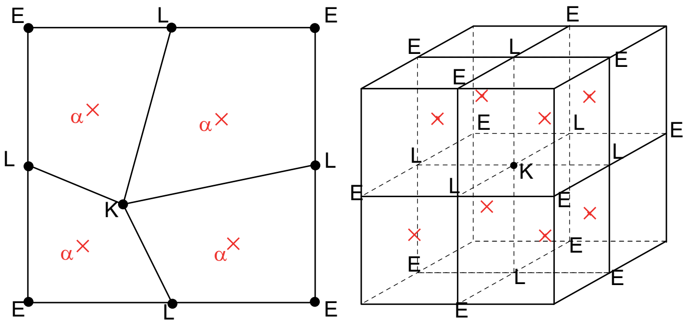

Fig. 3 The initial arrangement of the arbitrary node K in a grid in 2D (left) and 3D (right) used to illustrate the smoothing/remeshing methods described in Eq. (2-(10)

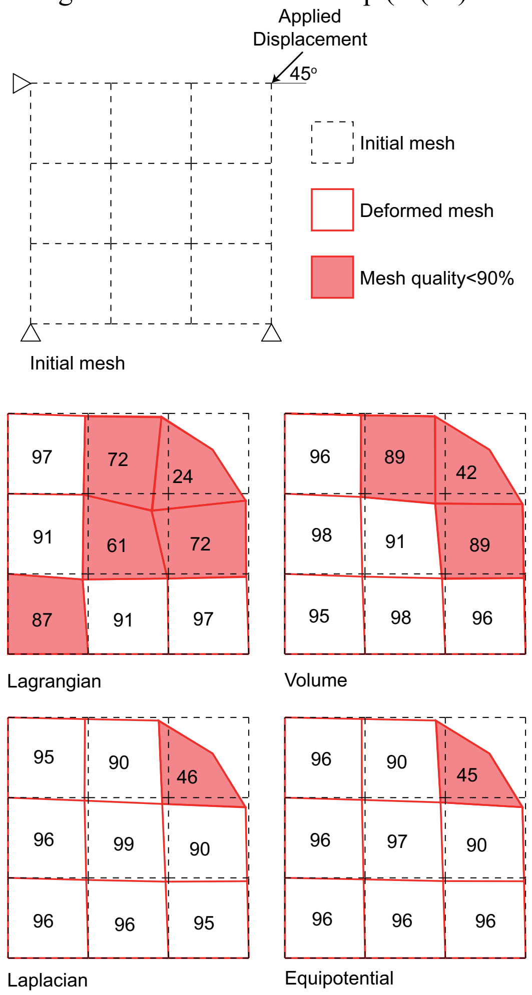

Fig. 4 Comparison of different smoothing/remeshing algorithms based on the achieved grid quality improvement (the numbers in the squares represents the Jacobian distortion index in percent), the elements colored with red have an element quality less than 90%

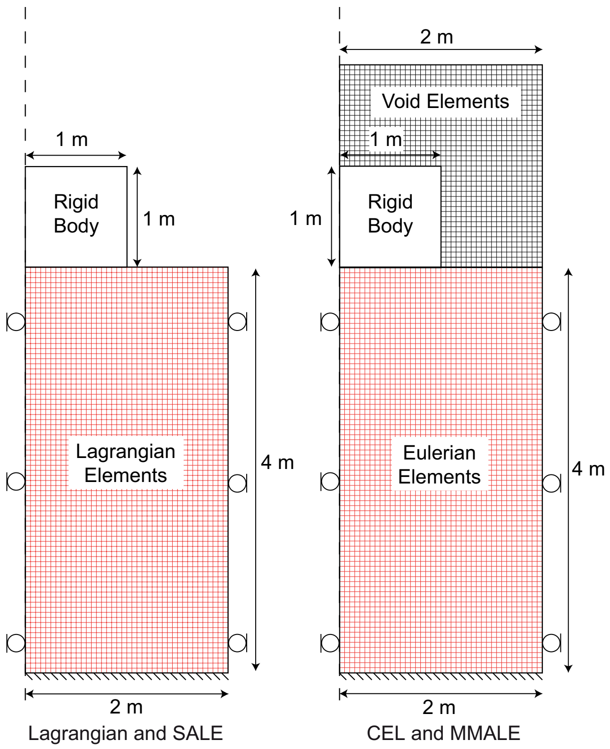

Fig. 5 Numerical mesh configuration of the strip footing problem (Bakroon et al., 2017)

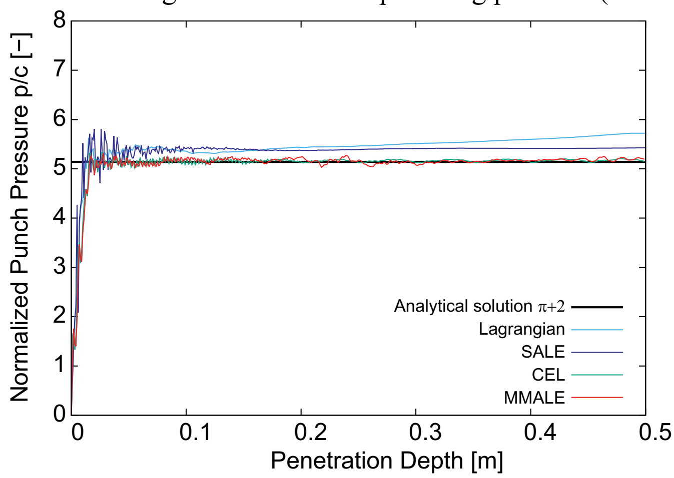

Fig. 6 Comparison of the punch pressure curves obtained from the Lagrangian, SALE, CEL, and MMALE with the analytical solution

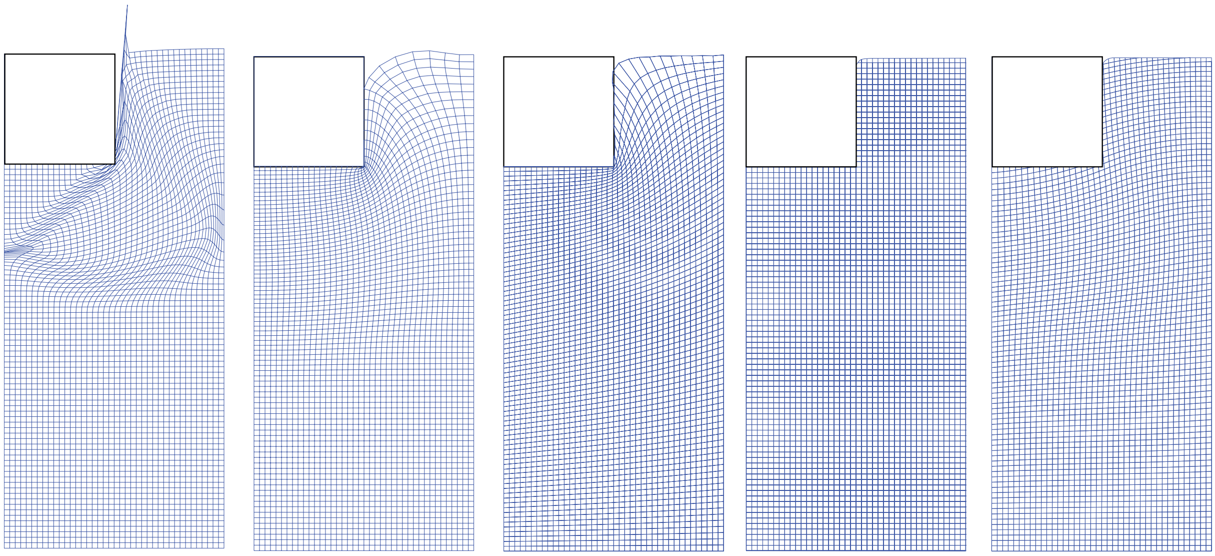

Lagrangian SALE - Volumetric SALE - Equipotential CEL MMALE

(a)

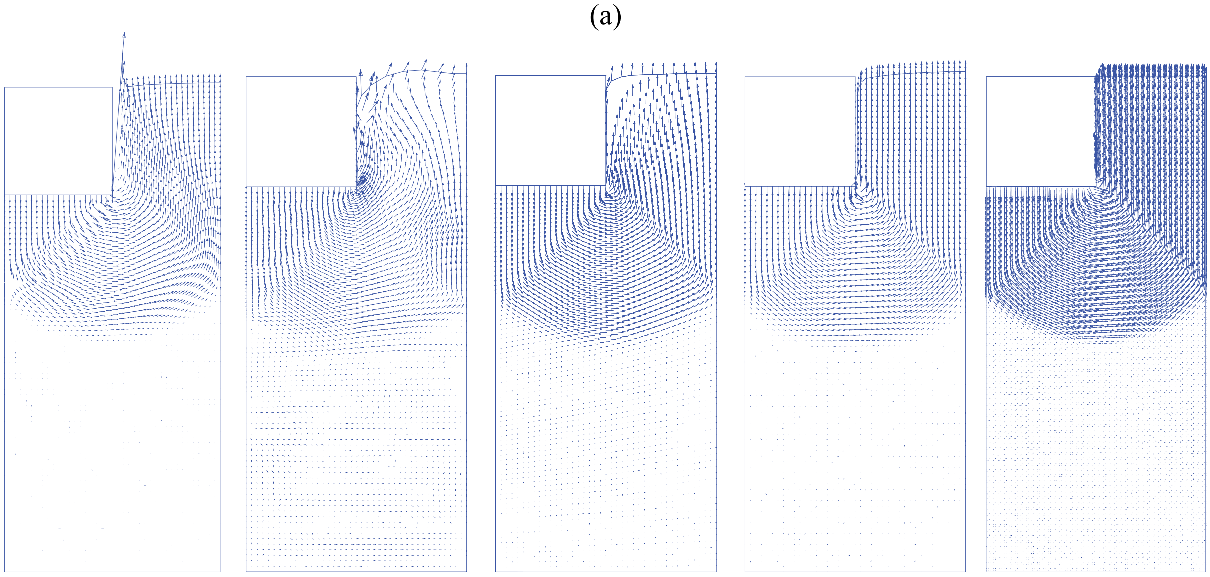

Lagrangian SALE - Volumetric SALE - Equipotential CEL MMALE

(b)

Fig. 7 (a) Mesh distortion and (b) velocity field after 0.5 m of strip footing penetration for different numerical methods

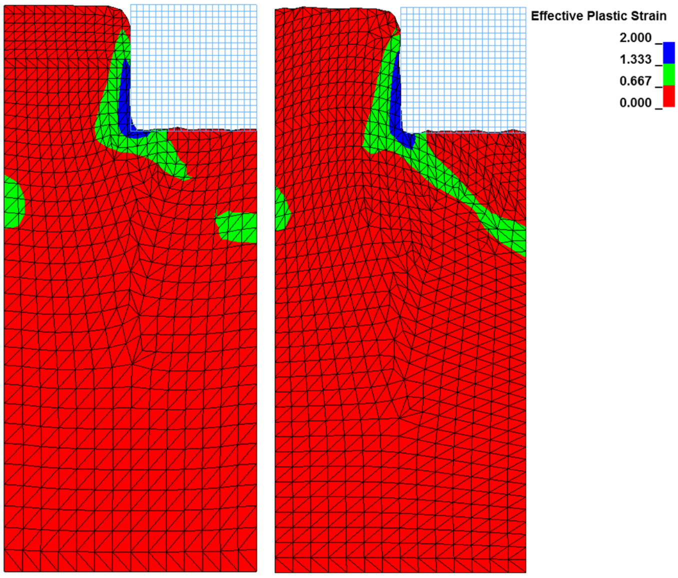

Fig. 8 The effective plastic strain after 0.5 m penetration for CEL (left) and MMALE (right)

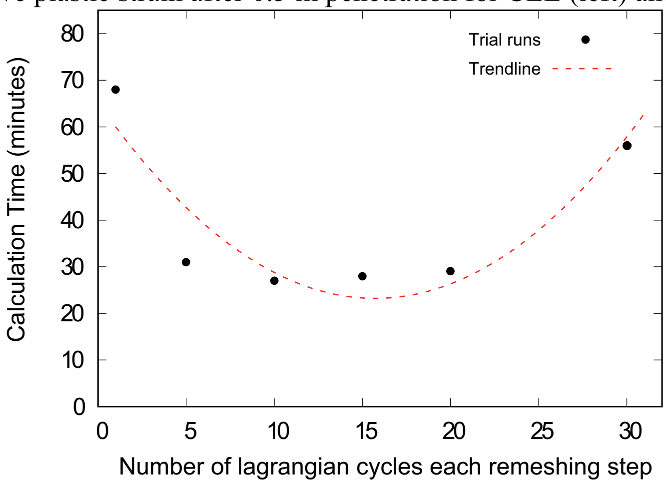

Fig. 9 MMALE time optimization achieved by changing the number of Lagrangian cycles in strip footing problem with 2.5-cm mesh element size

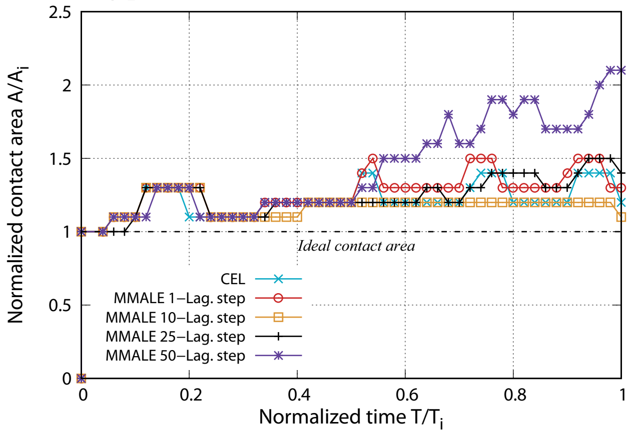

Fig. 10 Change in the normalized contact area during the simulation as a criterion to investigate leakage

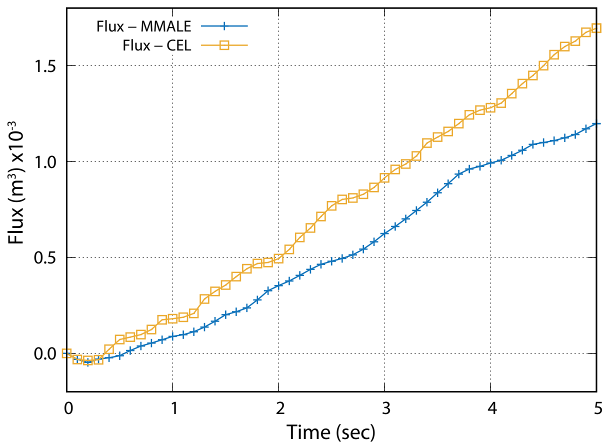

Fig. 11 The amount of material passed through the Lagrangian part (flux/leakage) during the simulation

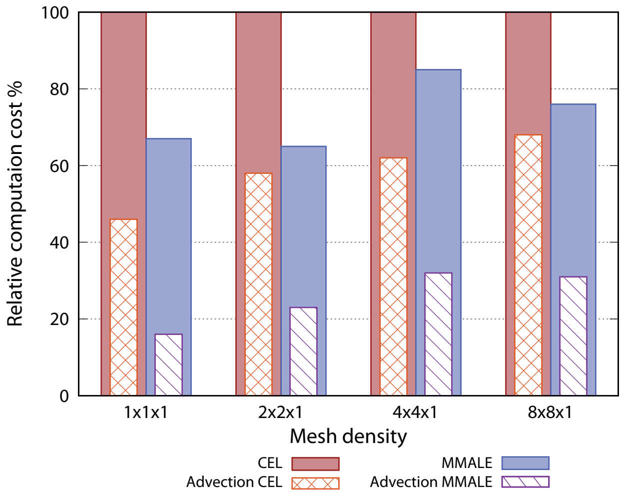

Fig. 12 Relative comparisons of computation costs between CEL and MMALE with their corresponding advection (The results are normalized according to those of CEL for each case)

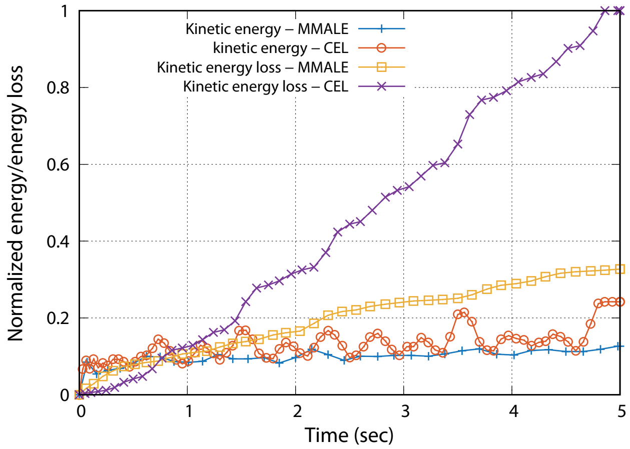

Fig. 13 Normalized kinetic energy and kinetic energy loss during the simulation for MMALE and CEL (the values are normalized with respect to the maximum value of kinetic energy loss curve for CEL)

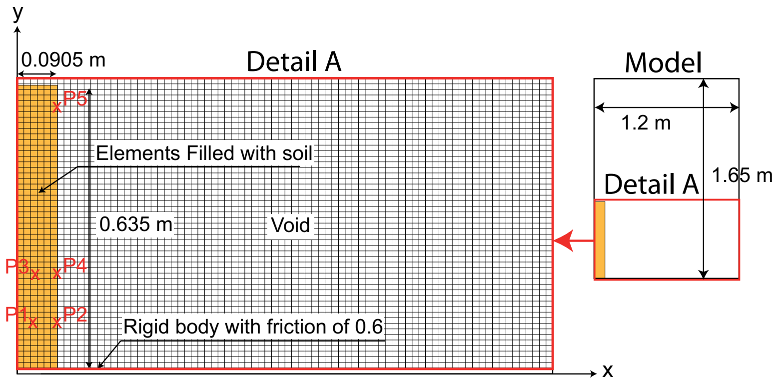

Fig. 14 Initial configuration of the numerical model for the case of CEL and MMALE; the model size is 1.65x1.2 m but only the mesh of the detail A is shown

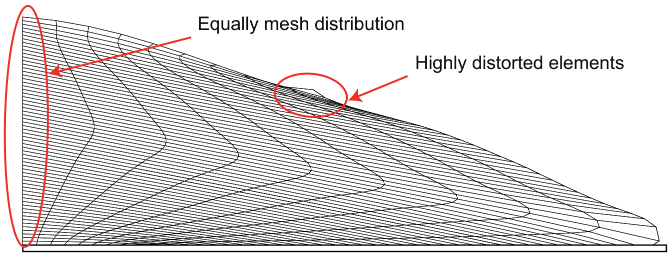

Fig. 15: Mesh deformation for Lagrangian and SALE simulations of sand column collapse

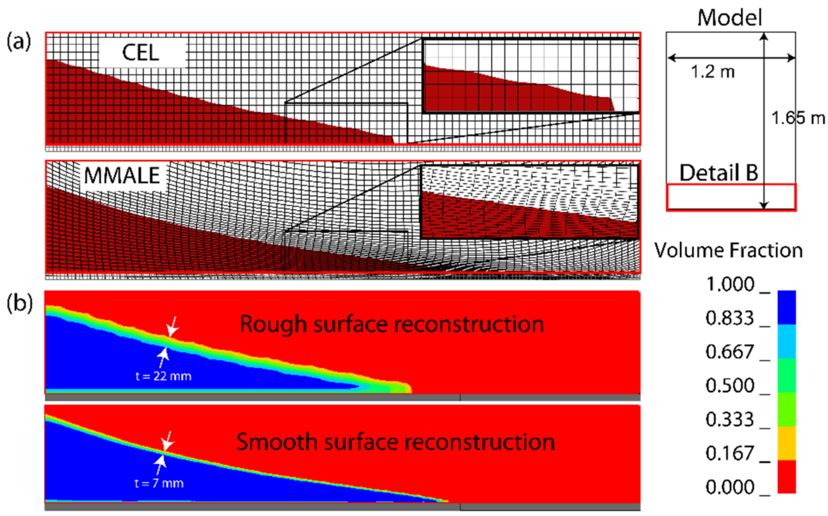

Fig. 16 (a) Final shape of the flowed soil as well as the mesh distortion in the sand column collapse for CEL (top) and MMALE (bottom), (b) Soil interface reconstruction in CEL (top) and MMALE (bottom), the contours represent the volume fraction of the soil in the elements; the results correspond to the detail B and not the whole model

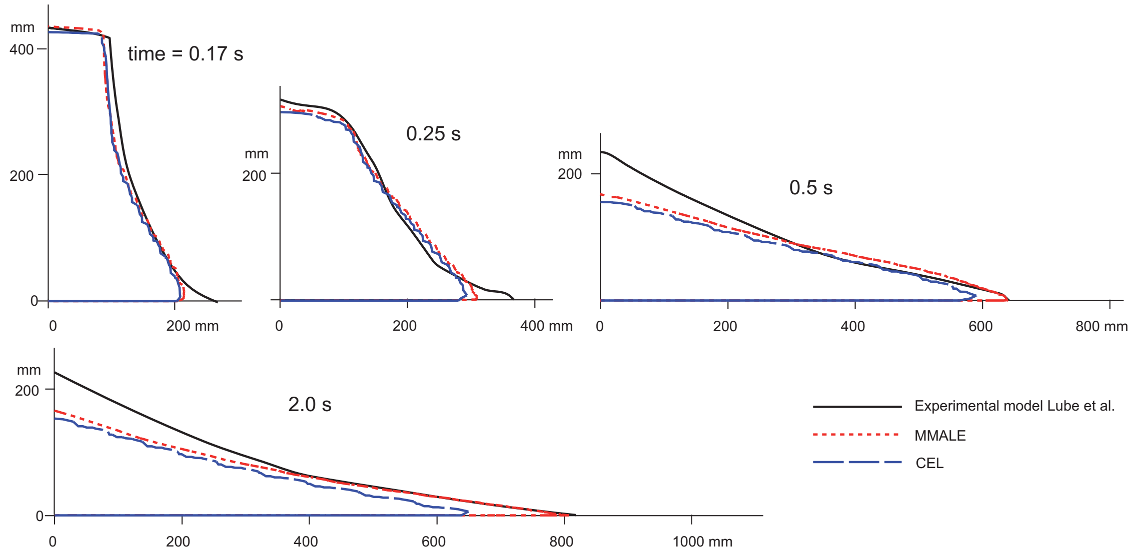

Fig. 17 Comparison of the run-out distance obtained from the numerical models with the experimental measurements in the sand column collapse problem

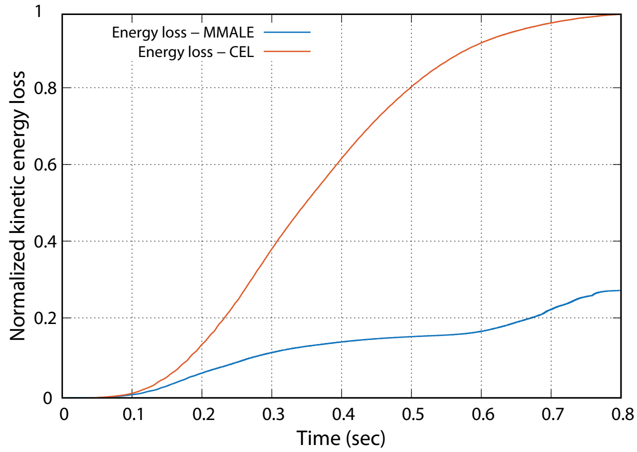

Fig. 18 Comparison of the normalized kinetic energy loss during advection for the sand column problem (the values are normalized with respect to the maximum value of CEL curve)

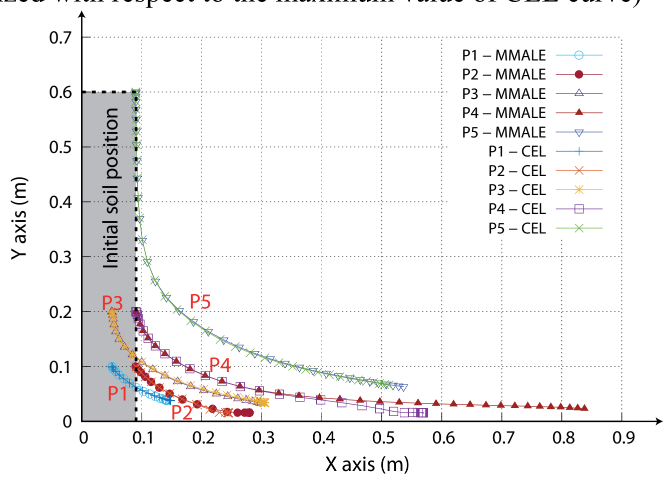

(a)

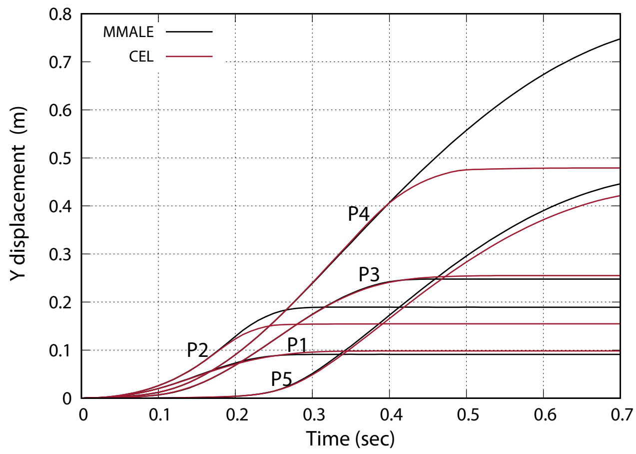

(b)

Fig. 19 (a) soil particle trajectory, (b) Comparison of the displacement between several particles obtained from CEL and MMALE

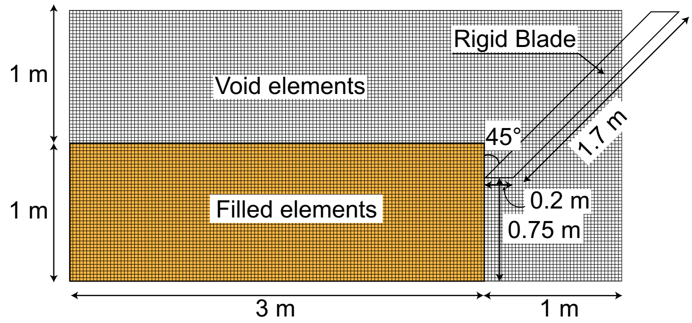

Fig. 20 Schematic view of the soil cutting problem

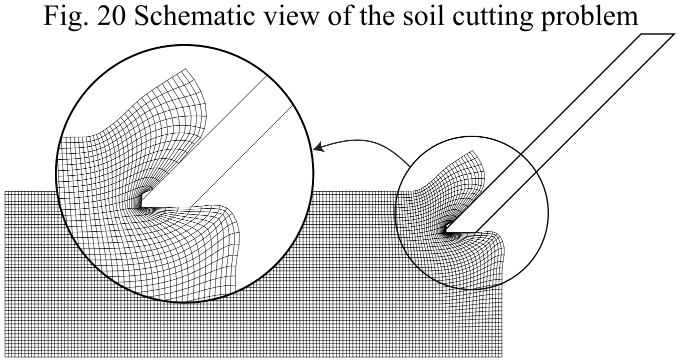

Fig. 21 Mesh distortion during the soil cutting using the SALE method

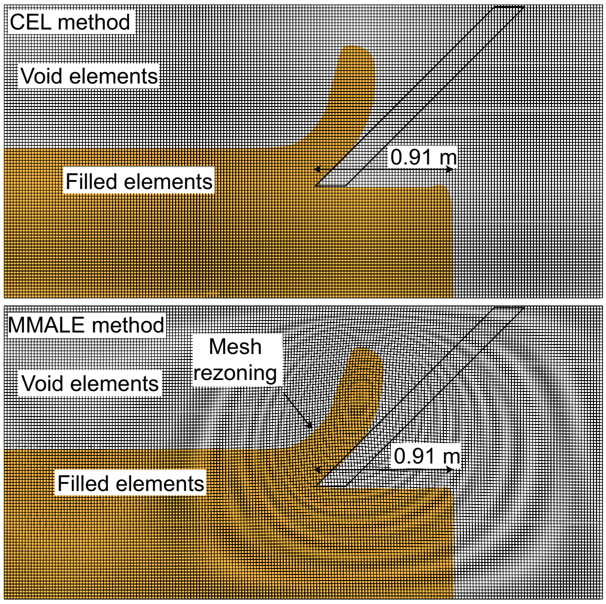

Fig. 22 Mesh distortion and soil deformation using CEL (above) and MMALE (below) methods in the soil cutting problem

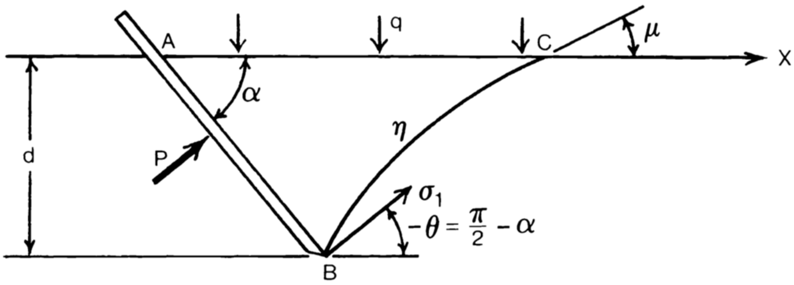

Fig. 23 Schematic of the assumed conditions in the soil cutting problem for deriving an analytical solution (McKyes, 1985)

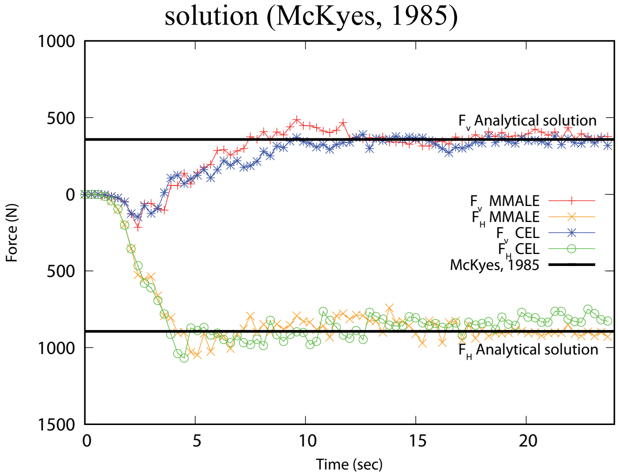

Fig. 24 Comparison of the induced horizontal and vertical forces on the blade obtained from MMALE and CEL methods with the analytical solution in the soil cutting problem

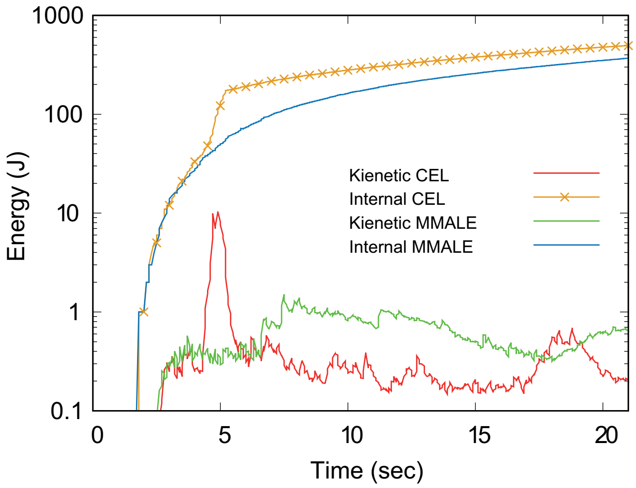

Fig. 25 Comparison of the internal and kinetic energy curves of the soil cutting problem

List of figure captions

Fig. 1 Schematic diagram of different grid-based approaches comparing the remeshing step effects on grid distortion level.

Fig. 2 Flowchart of the operator split scheme applied to the CEL and MMALE calculation steps

Fig. 3 The initial arrangement of the arbitrary node K in a grid in 2D (left) and 3D (right) used to illustrate the smoothing/remeshing methods described in Eq. (2-(10)

Fig. 4 Comparison of different smoothing/remeshing algorithms based on the achieved grid quality improvement (the numbers in the squares represents the Jacobian distortion index in percent), the elements colored with red have an element quality less than 90%

Fig. 5 Numerical mesh configuration of the strip footing problem Bakroon et al. (2017)

Fig. 6 Comparison of the punch pressure curves obtained from the Lagrangian, SALE, CEL, and MMALE with the analytical solution

Fig. 7 (a) Mesh distortion and (b) velocity field after 0.5 m of strip footing penetration for different numerical methods

Fig. 8 The effective plastic strain after 0.5 m penetration for CEL (left) and MMALE (right)

Fig. 9 MMALE time optimization achieved by changing the number of Lagrangian cycles in strip footing problem with 2.5-cm mesh element size

Fig. 10 Change in the normalized contact area during the simulation as a criterion to investigate leakage

Fig. 11 The amount of material passed through the Lagrangian part (flux/leakage) during the simulation

Fig. 12 Relative comparisons of computation costs between CEL and MMALE with their corresponding advection (The results are normalized according to those of CEL for each case)

Fig. 13 Normalized kinetic energy and kinetic energy loss during the simulation for MMALE and CEL (the values are normalized with respect to the maximum value of kinetic energy loss curve for CEL)

Fig. 14 Initial configuration of the numerical model for the case of CEL and MMALE; the model size is 1.65x1.2 m but only the mesh of the detail A is shown

Fig. 15: Mesh deformation for Lagrangian and SALE simulations of sand column collapse

Fig. 16 (a) Final shape of the flowed soil as well as the mesh distortion in the sand column collapse for CEL (top) and MMALE (bottom), (b) Soil interface reconstruction in CEL (top) and MMALE (bottom), the contours represent the volume fraction of the soil in the elements; the results correspond to the detail B and not the whole model

Fig. 17 Comparison of the run-out distance obtained from the numerical models with the experimental measurements in the sand column collapse problem

Fig. 18 Comparison of the normalized kinetic energy loss during advection for the sand column problem (the values are normalized with respect to the maximum value of CEL curve)

Fig. 19 (a) soil particle trajectory, (b) Comparison of the displacement between several particles obtained from CEL and MMALE

Fig. 20 Schematic view of the soil cutting problem

Fig. 21 Mesh distortion during the soil cutting using the SALE method

Fig. 22 Mesh distortion and soil deformation using CEL (above) and MMALE (below) methods in the soil cutting problem

Fig. 23 Schematic of the assumed conditions in the soil cutting problem for deriving an analytical solution McKyes (1985)

Fig. 24 Comparison of the induced horizontal and vertical forces on the blade obtained from MMALE and CEL methods with the analytical solution in the soil cutting problem

Fig. 25 Comparison of the internal and kinetic energy curves of the soil cutting problem